

# The Color Bimodality in Galaxy Clusters since $z \sim 0.9$ <sup>1,2</sup>

Yeong-Shang Loh

*Department of Physics and Astronomy, University of California, Los Angeles, CA 90095, USA*

yeongloh@astro.ucla.edu

E. Ellingson

*Center for Astrophysics and Space Astronomy, University of Colorado, Boulder, CO 80309, USA*

H.K.C. Yee and D.G. Gilbank

*Department of Astronomy and Astrophysics, University of Toronto, Toronto, ON M5S 3H4,  
Canada*

M.D. Gladders

*Department of Astronomy and Astrophysics, University of Chicago, Chicago, IL 60637, USA*

and

L.F. Barrientos

*Departamento de Astronomía y Astrofísica, Universidad Católica de Chile, Avenida Vicuña  
Mackenna 4860, Casilla 306, Santiago 22, Chile*

## ABSTRACT

We present the evolution of the color-magnitude distribution of galaxy clusters from  $z = 0.45$  to  $z = 0.9$  using a homogeneously selected sample of  $\sim 1000$  clusters drawn from the Red-Sequence Cluster Survey (RCS). The red fraction of galaxies decreases as a function of increasing redshift for all cluster-centric radii, consistent with the Butcher-Oemler effect, and suggesting that the cluster blue population may be identified with newly infalling galaxies. We also find that the red fraction at the core has a shallower evolution compared with that at the cluster outskirts. Detailed examination of the color distribution of blue galaxies suggests that they have colors consistent with normal spirals and may redden slightly with time. Galaxies of starburst spectral type contribute less than 5% of the increase in the blue population at high redshift, implying that the observed Butcher-Oemler effect is not caused by a unobscured starbursts, but is more consistent with a normal coeval field population.

*Subject headings:* methods: statistical – galaxies: elliptical and lenticular – galaxies: evolution – galaxies: clusters: general

## 1. Introduction

The comparison of local and high redshift clusters of galaxies is a powerful tool for constraining theories of structure formation and cosmological world models. The discovery that galaxy clusters at  $z \sim 0.5$  have a larger fraction of blue galaxies compared with similar clusters found in the local universe (Butcher & Oemler 1978, 1984) provided the first direct evidence of galaxy evolution in dense environments. Since these early studies, the Butcher-Oemler effect has been confirmed photometrically (Rakos & Schombert 1995; Margoniner & de Carvalho 2000; Margoniner et al. 2001; Kodama & Bower 2001; Goto et al. 2003) and spectroscopically (Dressler & Gunn 1982; Lavery & Henry 1988; Fabricant, McClintock & Bautz 1991; Dressler & Gunn 1992; Poggianti et al. 1999; Ellingson et al. 2001; Poggianti et al. 2006). This observed evolution has been interpreted variously as evidence for a rapid change in galaxy populations driven by ram-pressure stripping (Gunn & Gott 1972), galaxy-merging or other physical processes in clusters (Lavery & Henry 1988; Moore et al. 1996), as well as the effect of infalling galaxies from the field or near-field regions (Kauffmann 1995; Abraham et al. 1996; Ellingson et al. 2001).

However, the Butcher-Oemler phenomenon has been challenged from the start (e.g., Koo 1981) and more recently by a host of new analyses, drawn primarily from X-ray selected samples of clusters and near-infrared observation of galaxies (Andreon 1998; Andreon & Etti 1999; Smail et al. 1998; De Propris et al. 2003). In these, the evolutionary trend with redshift was found to be either weaker, or non-existent. The non-uniformity of the original Butcher-Oemler clusters, especially in physically related properties like galaxy surface number density (Newberry, Kirshner & Boroson 1988) and X-ray luminosity (Andreon & Etti 1999) may present selection biases that lead to a strong redshift evolutionary trend. Indeed, the original Butcher-Oemler clusters were selected from photographic plates and may include lower mass and unvirialized merging systems. The strong  $k$ -correction pushes the sample to bluer rest bands. These optically-selected galaxy samples may also preferentially select systems with strong star-formation (e.g., Gunn, Hoessel & Oke 1986; Andreon 2005).

Earlier studies also suffered from low number statistics. While the analyses were usually done

---

<sup>1</sup>based on observations carried out at the Canada-France-Hawaii Telescope (CFHT), operated by the National Research Council of Canada, the Centre National de la Recherche Scientifique of France and the University of Hawaii.

<sup>2</sup>based on observations taken at the Cerro Tololo Inter-American Observatory

with fewer than 50 clusters over a large lookback time (e.g., from  $z = 0$  to  $z = 0.5$ ), general claims were often made about the cluster population as a whole. Part of the reason is that investigators necessarily analysed whatever systems that were available. Uniformly selected cluster samples that span a large redshift range and have constant physical attributes (e.g., similar masses) are sparse and the variation of blue fraction within a fixed epoch is often considerable (e.g., Margoniner et al. 2001). It is unclear to what extent this variation is due to actual cosmic variance or the peculiarities of the sample selection itself, since the number of clusters involved is at most a few tens.

With the advent of wide area photometric and spectroscopic redshift surveys like the Sloan Digital Sky Survey (York et al. 2000, SDSS) and the Two-Degree Field Galaxy Redshift Survey (Colless et al. 2001, 2dFGRS), large catalogs of uniformly selected clusters are now available at low ( $z \sim 0.1$ ) to intermediate ( $z \sim 0.3$ ) redshift (e.g., Annis et al. 1999; Goto et al. 2002; Kim et al. 2002; Merchan & Zandivarez 2002; Eke et al. 2004; Yang et al. 2005; Merchan & Zandivarez 2005; Weinmann et al. 2006; Miller et al. 2005; Berlind et al. 2006). However, in order to understand what processes are dominant in explaining the Butcher-Oemler effect, a large redshift range is desirable to provide maximal leverage to evolutionary studies as various theoretical models may have different redshift dependences.

In this work, we revisit the Butcher-Oemler phenomenon using the currently largest sample of uniformly selected clusters of galaxies available, out to  $z \approx 0.9$ . The galaxy clusters are drawn from the complete and well-calibrated Red-Sequence Cluster Survey (RCS; Gladders & Yee 2005). The RCS method searches for galaxy overdensities along a color-magnitude sequence corresponding to cluster early-type galaxies, the cluster "red sequence". The apparent color of this sequence reddens with redshift, allowing us to separate overlapping structures and effectively remove most of the contamination that has plagued monochromatic cluster surveys. All massive clusters discovered by any methodology to date show a detectable red sequence, so that, while it is slightly less effective for very blue systems, this methodology is not expected to introduce a strong bias to the study of the cluster populations. To the extent that galaxies on the early-type red sequence have the largest fraction of stellar mass at a fixed luminosities (e.g., Bell et al. 2004), our cluster sample can be considered stellar mass dependent. Our sample may exhibit selection differences when compared, for example, with dark mass dependent weak lensing detected cluster samples such as the Deep Lens Survey (DLS; Wittman et al. 2002), intracluster medium (ICM) density dependent X-ray selected samples (e.g., Rosati et al. 1998), or star-forming galaxy biased blue overdensities for Lyman break selected samples. However, galaxy density maps derived from red sequence galaxies have been shown to correlate with weak lensing shear maps with high significance (Wilson, Kaiser & Luppino 2001).

In this paper we study the evolutionary trend of the red fraction for cluster galaxies with redshift within a range of radii, scaled by  $r/r_{200}$  – the radius at which the galaxy overdensity is 200

times the mean density. Scaling the radii to  $r/r_{200}$  allows a statistical combination of many systems and minimizes many problems arising from the foreground/background subtraction in photometric surveys. Our approach is cluster-centric (e.g., Melnick & Sargent 1977; Whitmore, Gilmore & Jones 1993; Ellingson et al. 2001), where we use a characteristic radius  $r_{200}$  to normalize the clusters across the richness range of the clusters. This approach is complementary to many more recent studies of the Color (Star Formation Rate)-Density relation (Hogg et al. 2003; Balogh et al. 2004; Yee et al. 2005) which use local galaxy densities (Dressler 1980; Smith et al. 2005; Postman et al. 2005; Cucciati et al. 2006; Cooper et al. 2007a).

The outline of this paper is as follows. In the next section, we describe the sample used in our analysis. The procedure for the statistical background correction of composite clusters is described in section 3. In section 4, we discuss our results and give caveats that need to be taken into account for robust interpretation. In section 5, we summarize our conclusions. Throughout this paper,  $h = H_0/100 \text{ km s}^{-1} \text{ Mpc}^{-1}$  and we adopt the concordance  $\Omega_m = 0.3, \Omega_\Lambda = 0.7$  cosmology.

## 2. Sample

### 2.1. The RCS Survey

The Red-Sequence Cluster Survey (RCS; Gladders & Yee 2005) is a  $\sim 100 \text{ deg}^2$  imaging survey in the  $z'$  and  $R_c$  bandpasses conducted with the CFHT 3.6 m and CTIO 4 m with the primary goal of searching for clusters of galaxies up to  $z \approx 1.4$ . There are 22 RCS patches (each of  $\approx 2.5 \text{ deg}^2$ ) distributed over the northern and southern sky. Some of the patches were chosen to overlap with other widely studied fields, such as XMM-LSS (Pierre et al. 2004), CDFS (Giacconi et al. 2001), CNOC2 (Yee et al. 2001), SWIRE (Lonsdale et al. 2003) and PDCS (Postman et al. 1996).

### 2.2. Photometry, Calibration, Extinction

The primary RCS photometric reduction of object detection, source deblending, star-galaxy separation and aperture photometry was performed using the Picture Processing Package (PPP; Yee 1991; Yee, Ellingson & Carlberg 1996). The detailed implementation of the RCS photometric pipeline is described in Gladders & Yee (2005). The average  $5\sigma$  limiting magnitudes for point sources are  $z' = 23.9$  and  $R_c = 25.0$  (AB system). Analysis of  $\log(N)$ - $\log(S)$  galaxy counts suggests that the photometry for extended sources is complete to  $\sim 0.8 \text{ mag}$  brighter, although there are variations from pointing to pointing. There are over 3 million point sources and 11

million galaxies in the RCS database. The relative photometry between patches is better than 0.1 magnitudes (Hsieh et al. 2005). Each detected extended source is further corrected for Galactic extinction, interpolating the dust map of Schlegel, Finkbeiner & Davis (1998) and assuming  $R_{R_c} = 2.634$  and  $R_{z'} = 1.479$ . For the present analysis, we use  $72 \text{ deg}^2$  of the RCS survey with the best photometry (Gladders et al. 2007). Throughout this paper, our  $R_c$  and  $z'$  photometry is presented on the AB system.

### 2.3. The Cluster Sample

About 8000 groups and clusters of galaxies were detected with high significance by searching for source overdensities in color slices along the red-sequence of early-type galaxies. Details of the cluster detection method are outlined in Gladders & Yee (2000). The release of the first catalog, as well as improvements over the cluster detection methodology, are described in Gladders & Yee (2005). A useful by-product of the red-sequence method is an estimated photometric redshift for each detected cluster. RCS uses only two bandpasses strategically chosen to straddle the  $4000\text{\AA}$  break of the target redshift coverage, and photometric redshifts of the detected clusters are quite well constrained, to  $\Delta z/z \approx 0.1$  (Gilbank et al. 2007). The dense collection of red galaxies along the red-sequence effectively diminishes the Poisson noise from photometric uncertainties of individual sources (López-Cruz, Barkhouse & Yee 2004).

In addition to an estimated photometric redshift (hereafter  $z_{\text{ph}}$ ), an optical richness parametrized by the amplitude of the galaxy-cluster cross-correlation function  $B_{\text{gc}}$  (Longair & Seldner 1979; Yee & Green 1987; Yee & Lopez-Cruz 1999) is measured.  $B_{\text{gc}}$  is found to correlate well with cluster properties such as X-ray temperature and galaxy velocity dispersion at intermediate redshift, and it is relatively well calibrated for X-ray selected clusters at  $z \sim 0.35$  (Yee & Ellingson 2003). Note that here we use red sequence galaxies for the measurement of  $B_{\text{gc}}$  (Gladders & Yee 2005), which gives a tighter relation with respect to X-ray properties, especially at higher redshift (Hicks et al. 2007). ROSAT observations have also found that most groups and lower mass systems with extended X-ray halos are dominated by early-type galaxies (Osmond & Ponman 2004; Mulchaey et al. 2003).  $B_{\text{gc}}$  computed from the red sequence will down-weight unvirialized poor systems without a hot ICM.

For the present analysis, we use  $\sim 1000$  clusters with  $B_{\text{gc}} > 300 (h_{50}^{-1} \text{ Mpc})^{1.77}$  and  $0.45 < z_{\text{ph}} < 0.90$ . Mass calibration using low to intermediate redshift clusters suggests these systems have richnesses corresponding to Abell Richness Class (ARC)  $\gtrsim 0$ ,  $\sigma_v > 450 \text{ km s}^{-1}$  and  $T_X > 3 \text{ keV}$  (Yee & Lopez-Cruz 1999; Yee & Ellingson 2003). The sample is divided into five redshift slices with 171 to 263 systems in each slice (Table 1). While the mass of each cluster is uncertain due to the rather large uncertainty in the measured  $B_{\text{gc}}$  and the intrinsic scatter in

mass- $B_{\text{gc}}$  relation, the overall distribution of cluster counts as a function of redshift is robust. Figure 1 shows the redshift histogram of clusters used in our analysis. Analysis of the RCS cluster counts to constrain cosmological parameters yields results consistent with the concordance values (Gladders et al. 2007), indicating that large systematic errors in our mass estimates are unlikely. From abundance matching, clusters with  $B_{\text{gc}} > 300 (h_{50}^{-1} \text{ Mpc})^{1.77}$  used in this paper are rare, with comoving densities  $< 10^{-5} h^3 \text{ Mpc}^{-3}$ , consistent with dark matter halos with mass  $\gtrsim 10^{14} h^{-1} M_{\odot}$ .

### 3. Methodology

#### 3.1. Foreground and Background Subtraction

To obtain the composite color-magnitude distribution of our cluster galaxies, we have to subtract the contribution from foreground and background galaxies statistically. The two-dimensional observed background counts for non-stellar sources in  $R_c - z'$  color and  $z'$  magnitude are constructed for each of the 22 RCS patches. Depending on the relative number of clusters from each patch used for the composite cluster analysis at each redshift slice, a weighted background based on the effective area contributed by the clusters is created (Figure 2). This semi-global background approach allows us to model the background more accurately using a large area, but still mimics some inherent patch to patch variations such as observing depth and seeing. This approach was similarly employed by Hansen et al. (2005) but performed in two dimensions (in color and magnitude space) as in Loh & Strauss (2006). Our approach is in contrast with Valotto, Moore & Lambas (2001) who advocate a local background subtraction methodology. Goto et al. (2003) find little difference with the two approaches if a large enough area is used. The global approach has the advantage that it uses all available data to constrain a smooth background with high precision. For a given patch of survey area, the region occupied by the clusters, after aggregating in redshift, takes up 2 – 5% of the entire patch area. We rescaled the background to match this total cluster area before the background subtraction.

We are interested in the average properties of clusters at a given redshift. If we assume that clusters are self-similar systems with a universal galaxy density profile, then clusters of different physical sizes can be scaled to some normalized cluster radius. However, without X-ray information or spectroscopy, it is difficult to measure the virial radius of each of the clusters. We use the measured  $B_{\text{gc}}$  for each cluster to estimate a virial radius  $r_{200}$  using the relation  $\log r_{200} = 0.48 \log B_{\text{gc}} - 1.10$ . This relation is empirically calibrated from intermediate redshift clusters (Yee & Ellingson 2003; Blindert 2006). We stack all clusters in a given redshift slice, but scale each cluster by its  $r_{200}$  for an effective normalizing scale. We emphasize here that  $B_{\text{gc}}$  is measured at the core, within  $0.25 h^{-1} \text{ Mpc}$ , and that the self-similar assumption is implicit in

Yee & Ellingson (2003). We note here that the spherical halo assumption inherent in the  $B_{\text{gc}}$  measurements is not perfect, as in addition to spherical distribution of red galaxies, the RCS method may systematically include physically associated filamentary galaxy structure along the line-of-sight. However, because of the overdensities implied at  $B_{\text{gc}} > 300 (h_{50}^{-1} \text{ Mpc})^{1.77}$ , most structures will be dynamically collapsed, if not completely virialized. We are exploring secondary measurements such as the concentration of the cluster galaxy distribution or the dominance of the BCG as a possible second parameter to further refine the mass measurements.

Figure 2 shows the color-magnitude distributions of galaxies with  $r/r_{200} < 0.5$  at  $z \approx 0.6$ . We have stacked 203 clusters with  $0.55 < z_{\text{ph}} < 0.65$  to obtain the observed distribution (left panel). The red sequence is clearly visible. The patch-weighted background distribution is shown next in the middle panel. The distribution after background subtraction is shown in the right panel. A prominent red sequence appears after the subtraction. The solid line is the fitted red sequence at the effective redshift. The solid dots indicate the model  $M^*$  at this redshift and the dashed vertical line indicates 1.5 magnitude fainter than  $M^*$ .

### 3.2. Semi-Empirical $k + e$ corrections

#### 3.2.1. Red Sequence $k + e$ models

When computing statistics like red (or blue) fractions across a range of redshifts, the use of an evolving luminosity limit is crucial since the absolute luminosity of galaxies changes by about one magnitude from  $z = 0$  to  $z \sim 1$ . The original Butcher & Oemler (1984) prescription of using a fixed rest-frame  $M_V = -20$  does not produce a consistent galaxy population across a range of redshifts. This bias is especially severe for studies which span a large redshift range. The known correlation between luminosity and color can also mimic the evolution of the blue fraction. However, there is considerable uncertainty in the measurement of luminosity evolution beyond  $z = 0.6$ . Work by Faber et al. (2005) and Bell et al. (2004) showed that DEEP2 and COMBO-17 surveys yielded very similar results out to  $z \sim 1$  with respect to the  $B$ -band luminosity density for red galaxies. However, Brown et al. (2007) and Scarlata et al. (2007) found a milder luminosity density evolution in the NOAO Deep Wide-Field and COSMOS surveys.

The luminosity function was determined empirically from background-subtracted galaxy counts in the red sequence of the clusters. A more detailed study of the RCS cluster luminosity function can be found in Gilbank et al. (2008); our assumed luminosity function is within 0.1 mag of the values listed in their Table I. These values of  $M^*$  (in the  $z'$  bandpass) as a function of redshift are consistent with the combination of  $k$ -correction for an early-type galaxy spectrum along with passive evolution from a  $z \sim 3$  single starburst population (see Gilbank et al. for details).

While our exact value of  $M^*$  may differ slightly from that measured by others, the evolution in  $M^*$  within our own sample is robust and will not influence trends with redshift. We explored the possible effects of uncertainty in the cluster galaxy luminosity function. A systematic change of  $\pm 0.25$  mag per redshift in  $M^*$  for the cluster galaxies produced a change in red fraction less than  $1\sigma$ .

Our goal is to obtain a consistent rest-frame flux for the cluster galaxies across the redshift range we are probing. We first use our model  $M^*$  to convert the apparent  $z'$  magnitudes of red sequence galaxies to evolution-corrected luminosities at the redshift of the cluster. The existence of the red sequence then allows us to match the color-luminosity distribution across redshift. The observed slope can be used to change the apparent  $R - z'$  color into units of  $C^*$  ( $R - z'$  color at  $M^*$ ), without appealing to model dependent color evolution (e.g., Bell et al. 2004; Loh & Strauss 2006). Figure 3 shows the color-luminosity distribution for two redshift slices:  $0.45 < z_{\text{ph}} < 0.55$  (first panel from the left) and  $0.85 < z_{\text{ph}} < 0.90$  (3rd panel). The axes are in units of  $M^*$  and  $C^*$ , the color relative to the red sequence.

### 3.2.2. Differential $k$ -correction

While model independent, the approach from the above section does not take into account the differential  $k$ -corrections between galaxies of different spectral types for a fixed observed  $z'$  magnitude. To this end, we use the observed color blue-ward of the red-sequence to infer the relative  $k$ -correction beyond the flux relative to a  $M^*$  at that epoch, which gives a comparable  $k + e$ -correction to more traditional approaches (e.g.,; Yee et al. 2005)

The left panel of Figure 4 shows the synthetic  $R_c - z'$  color for galaxies of different spectral types computed using *real* galaxy template spectra from Coleman, Wu & Weedman (1980) augmented with two starburst models. The empirically determined red-sequence color as a function of redshift is shown in red. Since the red sequence includes passive evolution of the stellar population, it does not match the non-evolving colors derived from local ellipticals at high redshift. Plotted on the right panel of Figure 4 are the synthetic colors, relative to the local ellipticals, for galaxies of different spectral type as a function of redshift. The y-axis can be compared directly with the y-axis of the red-sequence corrected color-magnitude distribution of Figure 3. From the relative color of each galaxy, we assign a spectral type to each, interpolating if the color is in between types. The relative  $k$ -correction in  $z'$ -band, used to shift a given galaxy to a lower intrinsic luminosity, is inferred from the differential  $k$ -correction relative to the fiducial red sequence template at each redshift.

Figure 3 shows the changes in the color-magnitude distributions before (1st and 3rd panels)



and after (2nd and 4th panels) applying the relative  $k$ -correction to the  $z'$ -band flux. This additional relative  $k$ -correction corrects blue galaxies for on-going star-formation by pushing them to fainter magnitudes, such that the bluest faint galaxies, which would otherwise just make our luminosity cut, are pushed below the magnitude limit and are so removed from our sample. This effect is clearly visible at higher redshift by examining blue galaxies in the 3rd and 4th panels of Figure 3 ( $0.85 < z_{\text{ph}} < 0.90$ ). The numerous blue galaxies brighter than  $M^*$  are corrected to fainter magnitudes but are still bright enough to be included in the sample. If we neglect the differential evolution between red sequence and blue galaxies, the derived red fraction at  $r_{200}$  is reduced by 2% at  $z \sim 0.5$  and by 14% at  $z \sim 0.8$ .

### 3.3. Cluster Red Fractions

There are a number of different ways in which red or blue galaxy fractions are defined in the literature. Some use a fixed rest-frame color cut, say rest-frame  $B - V < 0.8 \text{ mag}$  for blue galaxies (e.g., Rakos & Schombert 1995). Definitions like these usually yield a large number density evolution of early-type galaxies that are grossly inconsistent with the hierarchical model of structure formation (e.g., Wolf et al. 2003). Others, such as the original Butcher & Oemler (1984) studies, use a fixed color width  $\Delta$  from the observed red sequence, say,  $\Delta(B - V) = 0.2 \text{ mag}$  for red galaxies (e.g., Bell et al. 2004). As reviewed by Andreon (2005), a constant width bracketing the red sequence is not optimal because galaxies of different spectral types drift in and out of the fixed region  $\Delta$  for even the most generic models of stellar population. Claims of the evolution the blue (or red) fraction may just be a consequence of systematic spectral types drifting in and out of the width at different redshifts.

Here, we use an empirical approach that attempts to separate the red sequence galaxies from the rest of the population, and divide the remaining galaxies amongst different fixed spectral types. We first construct the  $k + e$  corrected  $R_c - z'$  color distribution by summing over the counts from all galaxies brighter than  $M^* + 1.5$ . The distribution for redshifts slices of  $0.45 < z_{\text{ph}} < 0.55$ ,  $0.65 < z_{\text{ph}} < 0.75$  and  $0.85 < z_{\text{ph}} < 0.90$  are shown on the bottom panels of Figure 5. We then fit the red side (split by the red sequence peak) of the distribution with a double Gaussian of a single mean, including a narrow peak and a broader wing. Because the intrinsic spread of the red sequence is small ( $\lesssim 0.05 \text{ mag}$ ; Bower, Lucey & Ellis 1992; Blakeslee et al. 2003; López-Cruz, Barkhouse & Yee 2004; Cool et al. 2006; Mei et al. 2006) and there should be on average no excess of galaxies with redder colors associated with these clusters, this half of the color profile should be characteristic of the color uncertainty in our observations and should be symmetric about the red sequence peak. This peak is prominent enough at all observed redshifts that red sequence galaxies are thus robustly isolated. The red fraction,  $f_R = 1 - f_B$ , the complement of the

traditionally measured blue fraction,  $f_B$ , is estimated by mirroring the double Gaussian about the mean model distribution, and normalizing by the total galaxy counts (red and blue, smoothed with a spline curve). We note here that our approach is in spirit similar to the original Butcher & Oemler (1984) studies where the color width of their red sequence galaxies was indeed  $\approx 0.2$  mag. This approach is also similar to the one suggested by Andreon (2005) of using the valley between the two distributions as a divider (e.g., Strateva et al. 2001) and more recent bi-gaussian fitting to the local field color distribution (at fixed luminosity) by Baldry et al. (2004). Our approach has the added advantage of estimating a more robust red fraction in the absence of a well-defined valley (e.g., the first distribution shown in Figure 5), and when there is a departure from bi-gaussianity. Furthermore, the observed red distribution seems to broaden at increasing redshift. Our approach automatically captures this broadening, presumably due to the larger photometric uncertainties of the individual sources at fainter apparent magnitudes. Both the valley division and the fixed width approach will not take this into account, creating a susceptibility to an Eddington-like bias (Eddington 1913) which might mimic the redshift evolutionary trend we are trying to detect.

### 3.4. Cluster-to-Cluster Variation

It has been noted from many previous studies of the Butcher-Oemler effect that even at fixed redshift, there is considerable variation in blue fraction. Some of this variation is due to the heterogeneous manner in which the clusters were selected, while others are intrinsic in the sense that even at a given epoch, clusters have various physical morphologies (e.g., Bautz-Morgan Class) and states of evolution. We try to capture this variation between clusters by performing a jackknife analysis on our stacked clusters at a given redshift slice. This is done by dividing the cluster sample further into 15 to 20 subsamples, depending on the number of clusters involved. Each subsample is then removed, and the same red fraction analysis is performed. The error-bars displayed in Figure 6 are obtained by this approach. We note here that this approach also captures other variations within our data set, like small residual differences in patch to patch relative photometry.

## 4. Results and Discussion

### 4.1. The Butcher-Oemler Effect

The cumulative red fraction as a function of redshift is shown in Figure 6. The fraction of red galaxies decreases as a function of redshift for all scaled radii  $r/r_{200}$ . Particularly relevant to the Butcher-Oemler phenomenon is the gradual decline in red fraction at the cluster core ( $0.25 r_{200}$ ) from  $\sim 95\%$  at  $z \approx 0.5$  to  $\sim 80\%$  at  $z \approx 0.9$ . The red fraction value of our lowest redshift bin

is high compared with the original Butcher & Oemler (1984) study and many subsequent analyses which showed red fractions of about 0.7 at  $z \sim 0.4$ . Part of this discrepancy comes from the way in which the red fraction is measured; using a fixed color cut in the bimodal distribution will tend to increase the blue fraction if the observational scatter is significant. Our values are more consistent with recent studies using X-ray-selected cluster samples at  $z \sim 0.3$  (Wake et al. 2005) and  $z \sim 0.6$  (Andreon, Lobo & Iovino 2004).

At face value, our result is inconsistent with the K-band analysis of De Propris et al. (2003) which probed a similar redshift range, but was based on a more massive (on average) and heterogeneous sample of 33 optical, X-ray and radio-selected clusters. They fitted their data with a constant  $f_B \sim 0.1$  out to  $z \sim 0.9$ . They confirmed the Butcher-Oemler effect as observed in an optically-defined sample, but noted little evolution when using a K-band selected sample. They concluded that any evolutionary effect may be due to a population of bursting dwarf galaxies, whose K-band luminosities (hence the stellar mass of the galaxies) are too faint for inclusion in a consistent K-band galaxy selection.

Our use of  $k + e$  corrected magnitude in the  $z'$ -bandpass is not a perfect proxy for galaxy stellar mass but is less affected by recent star formation and has a much smaller  $k + e$  correction compared with other optical bandpasses. Hence, we expect a reasonable agreement with K-band results. However, we find that our analyses differ significantly in the division of red versus blue galaxies. Like Butcher & Oemler (1984), De Propris et al. use a fixed  $\Delta(B - V) = 0.2$  mag but  $k$ -corrected to their observed bandpasses using an effective SED derived from Sa + Sc mixture to give an effective  $\Delta(\text{color})$  at higher redshift. Unlike Butcher & Oemler whose color histograms have an observed red sequence width of  $\approx 0.2$  mag, the color histograms from De Propris et al. display a narrower red sequence width compared with the effective  $\Delta(\text{color})$  – often as large as 0.5 mag – used in their analysis. Their chosen  $\Delta(\text{color})$  allows the inclusion of galaxies of later spectral type in the red fraction, suppressing their blue fraction measurements relative to ours, which model the observational scatter. On examination of the individual color histograms of their high redshift clusters, we find that our method would produce substantial blue counts beyond the red sequence, and hence we find no evidence of inconsistency between our results and theirs.

We further note that the De Propris et al.’s results are derived using a fixed aperture of relatively small size ( $0.25 - 0.45h^{-1}$  Mpc), whereas our red fractions are measured using apertures of scaled radii  $r/r_{200}$ . Observations made within a fixed metric radius tend to sample only the redder inner cores for massive clusters, and at  $z > 0.6$ , their sample is likely biased toward the most massive systems for which the  $r_{200}$  values are typically as large as  $1.5$  to  $2.0h^{-1}$  Mpc. As Figure 6 for the RCS sample shown, at radii smaller than  $0.5r_{200}$ , there is only a moderate evolution in the red fraction between  $z \sim 0.4$  and  $0.9$ .

Our definition of red fraction is sensitive to our assumption that the red sequence color spread

is symmetric, and dominated by observational uncertainties. This appears to be the case for most of our data. However, in our two lowest redshift slices  $0.45 < z_{\text{ph}} < 0.50$  and  $0.50 < z_{\text{ph}} < 0.55$ , we find that the chosen filters are not ideal separators of the red and blue distributions. In these two bins, the blue galaxies scatter underneath the red sequence so that our reflection of the red wing of the distribution will tend to oversubtract by a small amount. This effect is more problematic at fainter magnitudes because of the larger fraction of blue galaxies. For this redshift bin we fit the red sequence separately in four different magnitude bins to better separate the two distributions. Even so, the red fraction measured in this bin may be slightly too large by at most 5%. The problem only occurs in the lowest redshift slice, since at higher redshifts, the blue cloud is more widely separated in color space from the red peak for these filters. Inclusion of data from bluer filters will allow a better separation of the red and blue galaxies at the lower redshifts. An analysis using four color data (Hsieh et al. 2005) over a smaller area will be explored in a future paper.

## 4.2. Radial Dependence

A population gradient is seen for all redshifts in that the red fraction is larger in the cluster cores at all redshifts. In Figure 6 we plot the red fraction as a function of redshift for galaxies within  $r/r_{200} < 0.25$ ,  $0.25 < r/r_{200} < 0.50$ ,  $0.50 < r/r_{200} < 1.00$  and  $1.00 < r/r_{200} < 2.00$ . This result is similar to many low-redshift studies of clusters (e.g., Andreon et al. 2006; Goto et al. 2004; Ellingson et al. 2001). In their analysis, Goto et al. (2004) found a break at  $r/r_{200} \sim 0.3\text{--}0.8$  at their highest redshift bin ( $0.2 < z_{\text{ph}} < 0.3$ ). Our results indicate a similar change in the radial gradient of the red fraction at  $r/r_{200} \gtrsim 0.50$ . We caution such interpretations in light of the somewhat uncertain mass estimates of the clusters. Both statistical and systematic uncertainties in the cluster masses may affect our measures of the evolution of the red fraction and its radial dependence. Mass estimates from  $B_{\text{gc}}$  measurements have  $\sim 60\%$  uncertainties for individual systems, which translate to 30% uncertainties in  $r_{200}$ . Population gradients will be smoothed on this scale, possibly flattening any radial gradients on this scale, but most likely not affecting the comparison of evolution between  $0.25 r_{200}$  and  $1.00 r_{200}$ .

The decline in red fraction with redshift is significantly steeper in the outskirts ( $1.00 < r/r_{200} < 2.00$ ) compared to the core ( $r/r_{200} < 0.25$ ). Our results qualitatively agree with earlier work by Ellingson et al. (2001) and Kodama & Bower (2001) who found a milder decrease in red fraction at the core compared to the outskirts/field using an X-ray-selected clusters sample with spectroscopic redshifts. A possible interpretation is that this effect comes from a relative decline in the infall rates of bluer galaxies into clusters, as new additions to the cluster should generally lie at larger radii. We note that while systematic errors in our estimates of cluster masses, galaxy luminosity functions and  $k$ -corrections may affect our calculation of red fractions, this differential

effect with respect to radius will remain, suggesting that the population in the cores of clusters changes with time differently from the population in the outskirts.

Our result on the radial dependence of the red fraction requires an accurate determination of each cluster center. A detailed description for determining RCS cluster centers was given in Gladders & Yee (2005). In brief, the location of a cluster is first selected from the color- position data-cube with a magnitude weighting towards galaxies brighter than  $M^*$ ; the positioning is then refined by an iterative Gaussian kernel of  $250h^{-1}$  kpc. To the extent that the RCS algorithm is accurate, then the centering should be better than  $< 250h^{-1}$  kpc. Note that clusters in reality are not round objects and often there are double clusters, or galaxy overdensities along filamentary structures. If a cluster is indeed elliptical and has a well-defined center, we argue here that we will get the right center to better than half our searching scale (i.e.  $125h^{-1}$  kpc). If the cluster or galaxy overdensity is filamentary, then our assumption of self- similar spherical clusters breaks down. Indeed our results at  $r < 0.25r_{200}$  maybe affected by centering problems, but not for the larger radii. If we are not systematically deviating in our cluster center determination, then the jackknife procedure in our error calculation would capture the diversity and uncertainty of our red fraction determination.

Because cluster galaxy populations show such marked radial gradients, any systematic variations of the  $B_{gc} - r_{200}$  relation with redshift may also change our red fraction as a function redshift, with any systematic tendency to overestimate cluster masses leading to a trend towards a lower red fraction. However, a significant systematic is required: even if our estimates of  $r_{200}$  are off by a factor of 3 at  $z \sim 0.8$ , compared to  $z \sim 0.5$ , we would still see an evolution with redshift. Currently, no such redshift dependence is found in the RCS mass estimates when the same cluster sample is analysed using a global self-calibration procedure (e.g., Hu 2003; Majumdar & Mohr 2004) which reflects standard cosmological parameters (Gladders et al. 2007). Ongoing work is currently being done to calibrate the mass of a subset of high redshift clusters using X-ray (Hicks et al. 2007), multi-object spectroscopy (Gilbank et al. 2007; Barrientos et al., in prep), weak lensing analyses (Hoekstra et al., in prep.) and mid-IR (Ellingson et al., in prep.) observations to constrain any such biases.

### 4.3. The Blue Galaxy Distribution

Figure 7 shows the blue distribution of galaxies after removing the fitted red distribution. The shaded vertical bands are the expected color for galaxies of different (late) spectral type, ranging from Sab (far right) to starburst (SB; far left), synthesized using a single representative SED for each type (cf. Figure 4). The width of the band reflects the finite redshift range in each subsample and the color variation as the filters shift along the SED with redshift. The blue distribution,

when compared with spectral type, appears to change slightly with redshift, becoming bluer at higher redshifts. The broadening towards the red tail at the highest redshift sample may be due to photometric uncertainty ( $0.10 - 0.15$  mag), but this cannot account for the longer tail to the blue. We find that the median galaxy spectral type for non-red-sequence galaxies changes by approximately half a spectral type between  $z = 0.4$  and  $z = 0.9$ , (dashed line in Figure 7, and the series of six blue squares in the middle panel of Figure 4), and the fraction of blue galaxies with colors bluer than  $I_m$  increases from 10% to  $\approx 40\%$ , between redshifts 0.5 and 0.9. Studies of color bimodality in field galaxies (Strateva et al. 2001; Bell et al. 2004; Blanton 2006) suggest that field galaxies have colors consistent with slightly later types at these redshifts.

The Butcher-Oemler effect has been attributed by some studies to a population of very blue starburst galaxies in clusters at high redshift (e.g., Rakos & Schombert 1995; De Propriis et al. 2003). We investigate this possibility by examining the redshift behavior of the fractions of blue galaxies with colors bluer than  $I_m$  spectral type. The contribution from galaxies with spectral type similar to unobscured starbursts (we take the color mid-point between the two models) is  $< 5\%$ , even for the highest redshift slice. This is an upper bound because we expect leakages from the more abundant redder galaxies to the blue tail due to photometric errors. Looking fainter into the luminosity function ( $> M^* + 1.5$ ) would increase the contribution from galaxies with later spectral types, but we show that the Butcher-Oemler effect as detected here is not driven by low-mass starbursts, and includes a component of brighter galaxies with colors consistent with normal coeval field galaxies. Recently, works from Elbaz et al. (2007) and Cooper et al. (2007b) have found an increase in the number of bright blue, normal (i.e. not low mass or starburst) galaxies in high density environments at  $z = 1$  relative to  $z = 0$  (which they suggest may drive an inversion of the star-formation – density relation). Although our survey only probes rich clusters, our results suggest that the Butcher-Oemler effect is driven by normal galaxies, and are qualitatively consistent.

#### 4.4. Selection Effects from the Red Sequence Method

By construction, our clusters are selected based on the red sequence method using  $z'$  and  $R_c$  bandpasses, which will create a bias against finding clusters with very blue populations. Our measurement of the Butcher-Oemler effect may thus be considered to be a lower limit. However, we do not expect that such incompleteness will create a large additional effect. Simulations of cluster detection efficiency using the RCS method (Gladders 2002) show that the least massive clusters in our sample (corresponding to  $B_{gc} \approx 300 (h_{50}^{-1} \text{ Mpc})^{1.77}$ ) at  $z \sim 0.9$  are detected at high efficiency with red fractions as low as 0.55. If the red fraction dips to only 0.2, this efficiency drops to 50%. More massive clusters may be detected at 80% efficiency at a red fraction of 0.2. Since we

do not calculate red fractions for individual clusters here, we cannot use this to create a quantitative correction. However, these efficiencies are still significant even in the worst case scenarios, and average values lie significantly far away from the red fractions where we expect a selection bias to occur. Moreover, no other method for finding high redshift clusters has identified a sample which contains a large fraction of massive clusters with these very blue colors, and the overall number of clusters found in the RCS survey appears to be consistent with current cosmologies. Thus, we conclude that the problem of missing very blue clusters of galaxies is not overwhelming, and the Butcher-Oemler effect is not likely to be significantly stronger than observed. Because of our red-sequence selection criterion, there is a possibility that our sample may have a slight relative bias toward the redder systems at higher redshift. If this is the case, then the observed Butcher-Oemler effect would be a slight underestimate of the true evolution.

## 5. Summary and Conclusions

We use  $R_C$  and  $z'$  observations of a sample of  $\sim 1000$  clusters with masses greater than  $\sim 10^{14} h^{-1} M_\odot$  and  $0.45 < z_{\text{ph}} < 0.90$  from the Red-sequence Cluster Survey (Gladders & Yee 2005) to investigate the evolution of the color-magnitude relationship for cluster galaxies. We construct composite color-magnitude diagrams for a number of redshift bins and ranges of cluster-centric radii, using cluster photometric redshifts and a statistical background subtraction technique. We correct each galaxy color distribution for an empirically-determined estimate of the cluster luminosity function and  $k$ -corrections as a function of galaxy color, and investigate the bimodal distribution of excess galaxies in cluster fields. The large dataset and composite technique allows us to avoid many of the difficulties of previous investigations, where the luminosity and color evolution of different galaxy types and observational scatter blur the definitions of "red" and "blue" galaxies. Our analysis is informed by recent studies that the red sequence of galaxies is intrinsically narrow (e.g., Bower, Lucey & Ellis 1992), allowing us to fit an empirical description of the effects of observational scatter in our data, and separate galaxies in the red sequence from the rest of the cluster population.

We find a decrease in the fraction of red-sequence galaxies (increase in the blue fraction) in clusters across this redshift range, qualitatively consistent with the Butcher-Oemler effect. Our measurements are difficult to compare quantitatively with previous measures of the blue fraction, and tend to yield somewhat higher red fractions because of our correction for scatter in the red sequence and explicit  $k$ -corrections for blue galaxies. Because of this, our results indicate a milder evolution than some earlier studies (e.g., Butcher & Oemler 1984; Rakos & Schombert 1995), but a stronger evolution than that suggested by De Propriis et al. (2003) using a small heterogeneous sample with K-band photometry. Our results are more consistent with recent studies of X-ray

selected cluster samples (e.g., Wake et al. 2005). We argue that while the red sequence technique may miss some fraction of very poor, blue clusters, this effect is minor, and the Butcher-Oemler effect is unlikely to be significantly stronger than seen here. We see consistent radial gradients in clusters, in that red fractions are higher in clusters cores than within larger radii at all redshifts studied. We also find a mild differential in the rate at which populations evolve – more slowly within the inner cores of the clusters ( $r < 0.25 r_{200}$ ) than in the outer regions ( $1.00 < r/r_{200} < 2.00$ ), consistent with previous results at  $0.3 < z < 0.6$  (Ellingson et al. 2001; Kodama & Bower 2001; Andreon et al. 2006). This differential may indicate that cosmologically-driven infall of bluer galaxies into clusters may be partially responsible for the evolution in populations, as these galaxies will preferentially be found at larger radii. The decline in infall rates in low-density cosmologies then contributes to the decline in this population over time (Ellingson 2003).

The color distribution of non-red-sequence galaxies appears to be consistent with a population of normal spirals, and shows a gradual evolution in the median color with redshift. There is only a minor contribution from galaxies with colors similar to unobscured starbursts. This places robust limits on interpretations of the Butcher-Oemler effect as being driven by starbursting dwarf galaxies that subsequently fade dramatically in clusters (e.g., Rakos & Schombert 1995; De Propris et al. 2003). However, the two-color data used here is insufficient to address quantitatively the star formation rates in cluster galaxies, or assess the possibility that obscured starburst and post-starburst galaxies play an important role in the evolution of cluster populations (Poggianti et al. 1999). Additional studies of galaxy spectral energy distributions, morphologies and star formation rates are underway to trace the evolution of individual galaxies in clusters in this sample.

YSL and EE thank the National Science Foundation (NSF) grant AST-0206154 for support. The RCS project is supported by grants from the Canada Research Chair Program, NSERC, and the University of Toronto to H.K.C.Y. LFB’s research is partially supported by FONDECYT under proyecto 1040423 and Centro de Astrofísica FONDAP. YSL thanks Michael Strauss and John Stocke for discussions. We thank Kris Blindert for sharing the results of her analysis of the mass-richness relation of intermediate redshift RCS clusters in advance of publication.

## REFERENCES

- Abraham, R.G., et al., ApJ, 471, 694  
 Andreon, S., 1998, ApJ, 501, 533  
 Andreon, S., & Ettori, S., 1999, ApJ, 516, 647



- Andreon, S., Lobo, C., & Iovino, A., 2004, MNRAS,
- Andreon, S., 2005, in “The Fabulous Destiny of Galaxies: Bridging past and present”, Marseille, June 2005
- Andreon, S., et al., 2006, MNRAS, 365, 915
- Annis, J., et al., 1999, BAAS, 31, 1391
- Barrientos, L.F., et al., 2004, ApJ, 617, L17
- Bell, E.F., et al., 2004, ApJ, 608, 752
- Berlind, A.A., et al., 2006, ApJS, 167, 1
- Baldry, I.K., et al., 2004, ApJ, 600, 681
- Balogh, M.L., et al., 2004, ApJ, 615, L101
- Blakeslee, J.P., et al., 2003, ApJ, 596, L143
- Blanton, M.R., et al., 2003, ApJ, 594, 186
- Blanton, M.R., 2006, ApJ, 648, 268
- Blindert, K., 2006, PhD thesis, University of Toronto
- Bower, R.G., Lucey, J.R., & Ellis, R.S., 1992, MNRAS, 254, 589
- Brown, M.J.I., et al., 2007, ApJ, 654, 858
- Butcher, H., & Oemler, A.Jr., 1978, ApJ, 219, 18
- Butcher, H., & Oemler, A.Jr., 1984, ApJ, 285, 426
- Crawford, C.S., et al., 1999, MNRAS, 306, 857
- Coleman, G.D., Wu, C.-C., & Weedman, D.W., 1980, ApJS, 43, 393
- Colless, M., 1989, MNRAS, 237, 799
- Colless, M., et al., 2001, MNRAS, 2001, 328, 1039
- Cool, R.J., et al., 2006, AJ, 131, 736
- Cooper, M.C., et al., 2007a, MNRAS, 376, 1445

- Cooper, M.C., et al., 2007b, astro-ph/0706.4089
- Cucciati, O., et al., 2006, astro-ph/0612120
- De Propriis, R., et al., 2003, MNRAS, 342, 725
- De Propriis, R., et al., 2004, MNRAS, 351, 125
- Dressler, A., 1980, ApJ, 236, 351
- Dressler, A., & Gunn, J.E., 1982, ApJ, 270, 7
- Dressler, A., & Gunn, J.E., 1992, ApJS, 78, 1
- Eddington, A.S., 1913, MNRAS, 73, 359
- Eke, V.R., et al., 2004, MNRAS, 348, 866
- Elbaz, D., et al.(2007), astro-ph/0703653
- Ellingson, E., et al., 2001, ApJ, 547, 609
- Ellingson, E., 2003, Ap&SS, 285, 9
- Faber, S., et al., 2005, astro-ph/0506044
- Fabricant, D.G., McClintock, J.E., & Bautz, M.W., 1991, ApJ, 381, 33
- Giacconi, R., et al., 2001, ApJ, 551, 624
- Gilbank, D., et al., 2007, AJ, 134, 282
- Gilbank, D., et al., 2008, ApJ, 673, 742
- Gladders, M.D., et al., 1998, ApJ, 501, 571
- Gladders, M.D., & Yee, H.K.C., 2000, AJ, 120, 2148
- Gladders, M.D., 2002, Ph.D Thesis, University of Toronto
- Gladders, M.D., & Yee H.K.C., 2005, ApJ, 157, 1
- Gladders, M.D., et al., 2007, ApJ, 655, 128
- Gomez, P.L., et al., 2003, ApJ, 584, 210
- Goto, T., et al., 2002, AJ, 123, 1807

- Goto, T., et al., 2003, PASJ, 55, 739
- Goto, T., et al., 2004, MNRAS, 348, 515
- Gunn, J.E., & Gott, J.R.III, 1972, ApJ, 176, 1
- Gunn, J.E., Hoessel, J.G., & Oke, J.B., 1986, ApJ, 306, 30
- Hansen, S.M., et al., 2005, ApJ, 633, 122
- Hicks, A., et al., 2007, astro-ph/0710.5513
- Hogg, D.W., et al., 2003, ApJ, 585, L5
- Hsieh, B.C., et al., 2005, ApJS, 158, 161
- Hu, W., 2003, PRD, 67, 081304
- Kauffmann, G., 1999, MNRAS, 274, 153
- Kim, R.S.J., et al., 2002, AJ, 123, 20
- Kodama, T., & Bower, R.G., 2001, MNRAS, 321, 18
- Koo, D.C., 1981, ApJ, 251, L75
- Lavery, R.J., & Henry, J.P., 1988, ApJ, 330, 596
- Le Fevre, O., et al., 2003, proc. of IAU Symp. 216, Maps of the Cosmos, Sydney, July 2003  
Colless, M., Staveley-Smith, L. (Eds)
- Lewis, I., et al., 2002, MNRAS, 334, 673
- Lima, M., & Hu, W., 2005, PRD, 72, 3006
- Longair, M.S., & Seldner, M., 1979, MNRAS, 189, 433
- Loh, Y.-S., & Strauss, M.A., 2006, MNRAS, 366, 373
- Lonsdale, C.J., et al., 2003, PASP, 115, 897
- López-Cruz, O., Barkhouse, W.A., & Yee, H.K.C., 2004, ApJ, 614, 679
- Lubin, L.M., Oke, J.B., 2002, & Postman, M., AJ, 124, 1905
- Majumdar, S., & Mohr, J.J., 2004, ApJ, 613, 41

- Margoniner, V.E., & de Carvalho, R.R., 2000, *AJ*, 119, 1562
- Margoniner, V.E., et al., 2001, *ApJ*, 548, L143
- Mei, S., et al., 2006, *ApJ*, 639, 81
- Melnick, J., & Sargent, W.L.W., 1977, *ApJ*, 215, 401
- Merchan, M.E., & Zandivarez, A., 2002, *MNRAS*, 335, 216
- Merchan, M.E., & Zandivarez, A., 2005, *ApJ*, 630, 759
- Miller, C.J., et al., 2005, *AJ*, 130, 968
- Moore, B., et al., 1996, *Nature*, 379, 613
- Motl, P.M., et al., 2005, *ApJ*, 623, L63
- Mulchaey, J.S., et al., 2003, *ApJS*, 145, 39
- Newberry, M.V., Kirshner, R.P., & Boroson, T.A., 1988, *ApJ*, 335, 629
- Osmond, J.P.F., & Ponman, T.J., 2004, *MNRAS*, 350, 1511
- Pierre, M., et al., 2004, *JCAP*, 09, 011
- Poggianti, B.M., et al., 1999, *ApJ*, 518, 576
- Poggianti, B.M., et al., 2006, *ApJ*, 642, 188
- Popesso, P., et al., 2005, *A&A*, 433, 415
- Postman, M.P., et al., 1996, *AJ*, 111, 615
- Postman, M., et al., 2005, *ApJ*, 623, 731
- Rakos, K.D., & Schombert, J.M., 1995, *ApJ*, 439, 47
- Rosati, P., et al., 1998, *ApJ*, 492, L21
- Scarlata, C., et al., 2007, *ApJS*, 172, 494
- Schechter, P., 1976, *ApJ*, 203, 297
- Schlegel, D.J., Finkbeiner, D.P., & Davis, M., 1998, *ApJ*, 500, 525
- Smail, I., et al., 1998, *MNRAS*, 293, 124

- Smith, G., et al., 2005, ApJ, 620, 78
- Strateva, I., et al., 2001, AJ, 122, 1861
- Valotto, C.A., Moore, B., & Lambas, D.G., 2001, ApJ, 546, 157
- Wake, D., et al., 2005, ApJ, 627, 186
- Weinmann, M.S., et al., 2006, MNRAS, 366, 2
- Whitmore, B.C., Gilmore, D.M., & Jones, C., 1993, ApJ, 407, 489
- Wilson, G., Kaiser, N., & Luppino, G.A., 2001, ApJ, 556, 601
- Wittman, D., et al., 2002, Proc. SPIE Vol. 4836
- Wolf, C., et al., 2003, A&A, 401, 73
- Yang, X., et al., 2005, MNRAS, 356, 1293
- Yee, H.K.C., & Green, R.F., 1987, ApJ, 319, 28
- Yee, H.K.C., 1991, PASP, 103, 396
- Yee, H.K.C., Ellingson, E., & Carlberg, R.G., 1996, ApJS, 102, 269
- Yee, H.K.C., & Lopez-Cruz, O., 1999, AJ, 117, 1985
- Yee, H.K.C., et al., 2000, ApJS, 129, 475
- Yee, H.K.C., & Ellingson, E., 2003, ApJ, 585, 215
- Yee, H.K.C., et al., 2005, ApJ, 629, L77
- York, D.G., et al., 2000, AJ, 120, 1579

Table 1:

redshift range	Number of Clusters
$0.45 < z < 0.55$	171
$0.55 < z < 0.65$	203
$0.65 < z < 0.75$	229
$0.75 < z < 0.85$	263
$0.85 < z < 0.90$	118

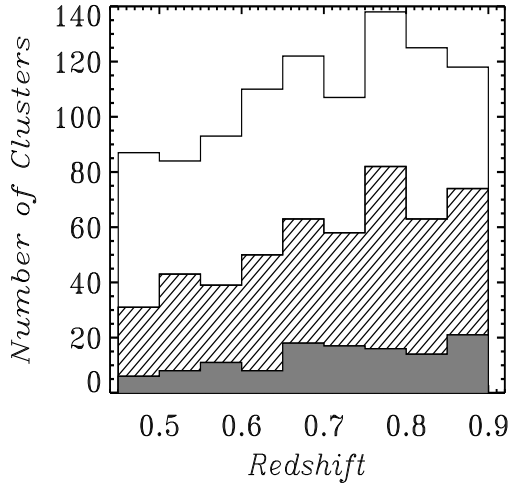


Fig. 1.— The redshift histogram of RCS clusters used in our analysis. The three segments indicate richness bins of  $B_{gc} > 800$  (grey for rich clusters),  $500 < B_{gc} < 800$  (hatched) and  $300 < B_{gc} < 500$  (white for poor clusters).

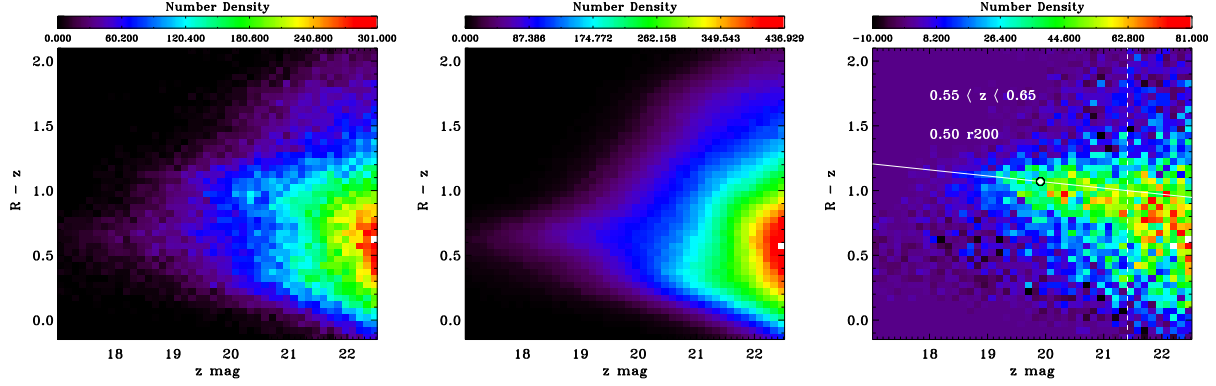


Fig. 2.— (Left) The observed color-magnitude distribution for all non-stellar sources with  $r < 0.5 r_{200}$  for 203 clusters with  $0.55 < z_{\text{ph}} < 0.65$ . (Middle) Patch-weighted background distribution (see text). (Right) Background-subtracted distribution of galaxies, calculated from the two preceding panels. The white dot indicates  $M^*$  at the median redshift ( $\sim 0.61$ ) while the dashed vertical line indicates  $M^* + 1.5$ , the consistent flux limit used for the red fraction analysis. The completeness of the photometry for extended sources ( $z' < 23.1$  and  $R_c < 24.2$ ) lies beyond the boundary of these figures.

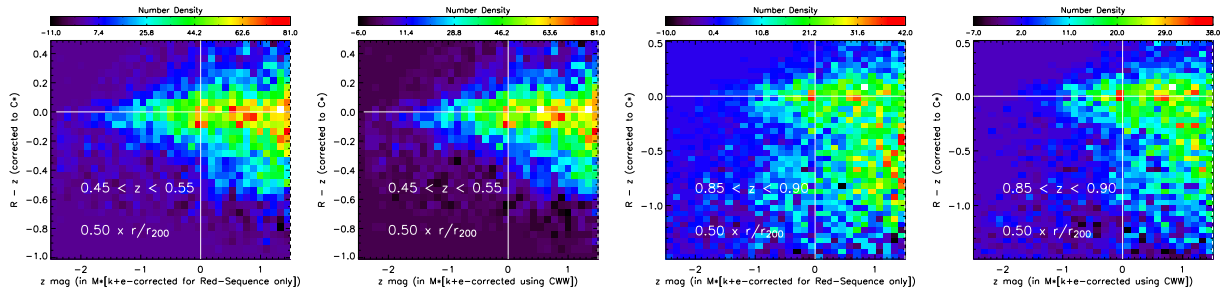


Fig. 3.— Color-magnitude distribution after  $k + e$  correction for  $0.45 < z_{\text{ph}} < 0.55$  (1st and 2nd panel from the left) and  $0.85 < z_{\text{ph}} < 0.90$  (3rd and 4th). The axes of the plots are in units of  $M^*$  and  $C^*$  at their respective redshifts. In the 1st and 3rd panel, the  $z'$ -band flux is corrected consistently for red sequence galaxies only. In the 2nd and 4th panel, a differential  $k$ -correction is based on the expected color of galaxies of different spectral type. This latter correction not only tightens the red sequence at low redshift, but also substantially reduces the counts of blue  $M < M^*$  galaxies at high redshift.

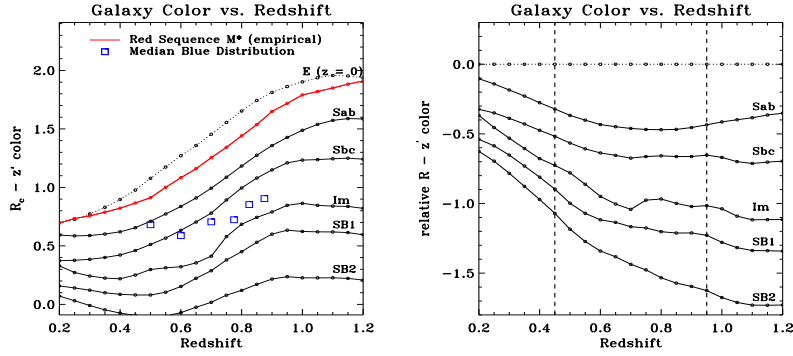


Fig. 4.— (Left) Synthetic  $R_c - z'$  colors for galaxies of different spectral type computed using galaxy template spectra from Coleman, Wu & Weedman (1980) and model starburst (SB1, SB2) galaxy spectra. The evolving red-sequence  $M^*$  model is shown in red. The series of squares are the median color of the non-red-sequence galaxies from RCS clusters (see section 4.3 and Figure 7) as a function of cluster redshift. (Right) Synthetic colors relative to a fiducial  $\sim M^*$  elliptical galaxy as a function of redshift. The y-axis is in units of  $C^*$ , the color relative to the colors of ellipticals from the CWW models. The vertical dashed lines bracket the redshift range of our sample.



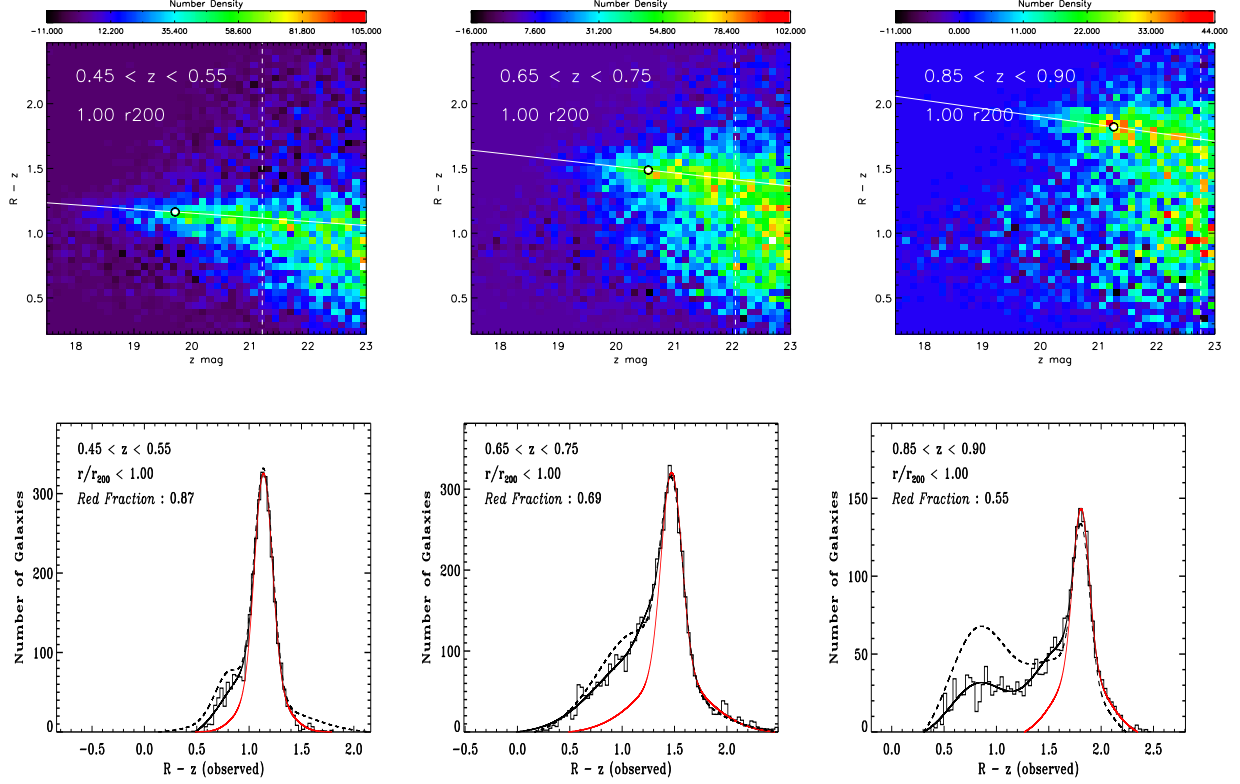


Fig. 5.— The top panels are the background subtracted color-magnitude distributions. The bottom panels are the color distribution after  $k + e$  correction. The histogram and the solid line shows the distribution after applying a differential  $k$ -correction for non-red sequence galaxies (see section 3.2.2) while the dashed lines show the distribution before such a correction was made. The red curve is our model for the red distribution used to compute the red fraction. The plots for are redshift slices:  $0.45 < z_{\text{ph}} < 0.55$  (left),  $0.65 < z_{\text{ph}} < 0.75$  (middle) and  $0.85 < z_{\text{ph}} < 0.90$  (right).

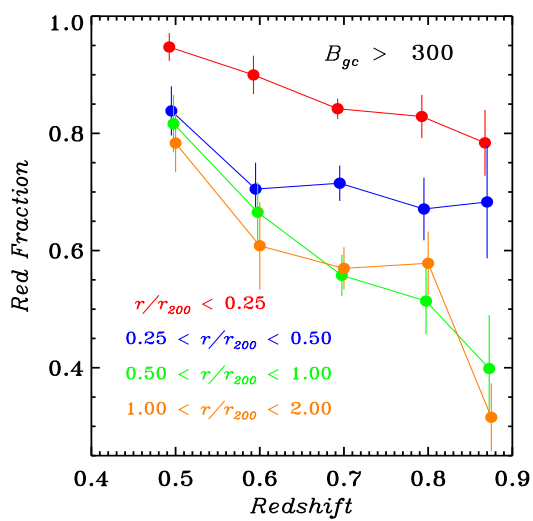


Fig. 6.— The red fraction as a function of redshift for galaxies with  $r/r_{200} < 0.25$  (core),  $0.25 < r/r_{200} < 0.5$ ,  $0.5 < r/r_{200} < 1.0$  and  $1.0 < r/r_{200} < 2.0$  (outskirts) and brighter than  $M^* + 1.5$ .

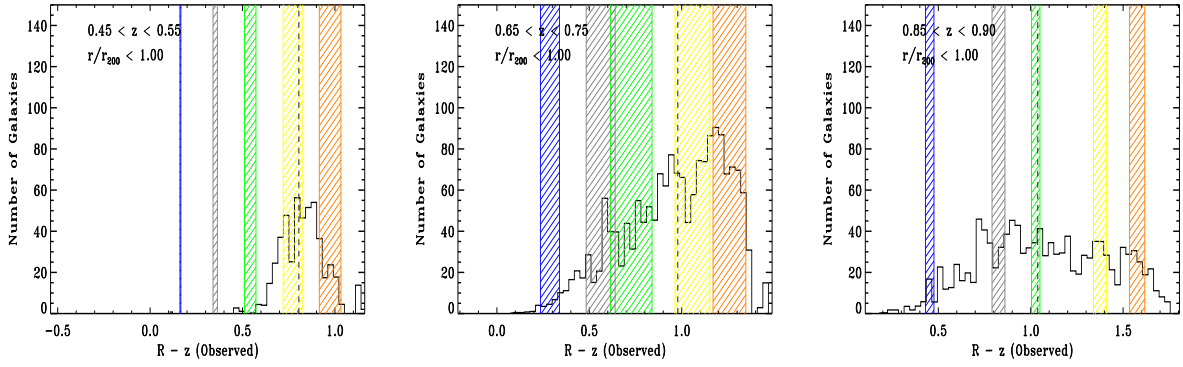


Fig. 7.— The blue distributions of galaxies after correction for the red sequence (solid histograms). The shaded bands in each plot are the expected color for different spectral types, ranging from Sab (far right), Sbc, Im, and starburst (SB1, SB2; far left), synthesized using a single representative SED for each type (see text). The width of the band reflects the finite redshift range in each subsample and the color variation as the filters shifts along the SED with redshift. The plots are for redshift slices:  $0.45 < z_{\text{ph}} < 0.55$  (left),  $0.65 < z_{\text{ph}} < 0.75$  (middle) and  $0.85 < z_{\text{ph}} < 0.90$  (right). The vertical dashed lines indicate the median colors of the distributions, also plotted in Figure 4.